Graphene Field-Effect Transistors with Ferroelectric Gating

Yi Zheng,[1,2,*] Guang-Xin Ni,[1,3,*] Chee-Tat Toh,[1] Chin-Yaw Tan,[3] Kui Yao,[3] and Barbaros Özyilmaz[1,2,4,*,†]

[1]*Department of Physics, 2 Science Drive 3, National University of Singapore, Singapore 117542*
[2]*NanoCore, 4 Engineering Drive 3, National University of Singapore, Singapore 117576*
[3]*Institute of Material Research and Engineering (IMRE), 3 Research Link, Singapore 117602*
[4]*NUS Graduate School for Integrative Sciences and Engineering (NGS), Singapore 117456*

(Received 11 March 2010; published 11 October 2010)

Recent experiments on ferroelectric gating have introduced a novel functionality, i.e., nonvolatility, in graphene field-effect transistors. A comprehensive understanding in the nonlinear, hysteretic ferroelectric gating and an effective way to control it are still absent. In this Letter, we quantitatively characterize the hysteretic ferroelectric gating using the reference of an independent background doping (n_{BG}) provided by normal dielectric gating. More importantly, we prove that n_{BG} can be used to control the ferroelectric gating by unidirectionally shifting the hysteretic ferroelectric doping in graphene. Utilizing this electrostatic effect, we demonstrate symmetrical bit writing in graphene-ferroelectric field-effect transistors with resistance change over 500% and reproducible no-volatile switching over 10^5 cycles.

DOI: 10.1103/PhysRevLett.105.166602 PACS numbers: 72.80.Vp

The electric field effect, which continuously tunes the Fermi level (E_F) in the conical energy band structure of graphene, plays a critical role in studying the extraordinary electronic properties of graphene [1]. By using conventional dielectrics such as SiO_2 and more recently HfO_2, poly(methyl methacrylate), and Al_2O_3 with linear dielectric response to an electric field, many fascinating physics have been discovered. Among these celebrated phenomena are the anomalous quantum Hall effect [2], Klein tunneling [3], and the gate-tunable band gap in bilayer graphene [4]. Despite such tremendous progress, there is keen interest in the science community to utilize new dielectrics and substrates for exploring new graphene physics and functionalities [5–9]. Among promising candidates, ferroelectrics are unique both in ultrahigh dielectric constants (κ) up to a few thousands and nonlinear, hysteretic dielectric response to an electric field. The ultrahigh κ makes ferroelectrics promising substrates for studying the charge scattering mechanism in graphene [10–13], which could be a crucial step in realizing ultrahigh mobility [14] in nonsuspended graphene. Equally important, the ultrahigh κ may allow ultrahigh doping in graphene with charge densities ($> 10^{14}$ cm^{-2}) exceeding electrolyte doping [15] *and* with gate tunability at cryogenic temperatures. Based on the hysteretic ferroelectric gating, a novel functionality of nonvolatile graphene-ferroelectric field-effect transistors (GFeFETs) has been demonstrated [16].

However, the fundamental understanding of ferroelectric gating is still elusive. In contrast to the linear doping vs normal dielectric gating relation $n = \alpha Vg$ [1], ferroelectric gating introduces a pronounced hysteresis in the charge doping. In particular, polymer ferroelectric gating introduces strong electron-hole puddles in graphene even far away from the Dirac point. Therefore, Hall measurements alone may be misleading in determining the induced charge doping (see supplemental material [17]). Thus, a quantitative modeling will not only improve the understanding of ferroelectric gating but also help in optimizing the performance of GFeFETs. Ferroelectric gating is also characterized by two symmetrical remnant polarizations, i.e., $P_\uparrow = P_r$ and $P_\downarrow = -P_r$ for upwards and downwards dipole configurations, respectively. Consequently, $P_\uparrow$ and $P_\downarrow$ induce two *identical* zero-field resistance states in graphene. Although two distinct resistance states can be created by polarizing [$R_0(P_r)$] and depolarizing [$R_1(P \approx 0)$] the ferroelectric thin film alternately [16], the depolarization state is not in thermodynamic equilibrium and less stable than the polarization state. To solve this problem, we need an effective way of controlling the hysteretic ferroelectric doping. Last but not least, GFeFETs in our earlier work [16] are characterized by low charge carrier mobility of a few hundred cm^2 V^{-1} s^{-1}. Such low mobility prevents the determination of the intrinsic physical properties and limitations of GFeFETs.

In this Letter, we present a quantitative understanding of high quality graphene devices under ferroelectric gating. For this purpose, we introduce an independent reference doping (n_{BG}) by the SiO_2 back gating. We show that the evolution of the device resistance hysteresis from symmetrical double peak to asymmetrical single peak structures can be consistently simulated by the electric displacement continuity equation using the reference of the SiO_2 gating. We also show that, by controlling the polarity and magnitude of n_{BG}, the hysteretic ferroelectric doping in graphene can be shifted unidirectionally. In analogy to exchange biased spin valves [18], this effect provides a reference point for maximizing the resistance change at zero electric field and enables symmetrical bit writing in GFeFETs. We demonstrate highly reproducible nonvolatile switching over 10^5 cycles and $\Delta R/R$ exceeding 500% in GFeFETs.

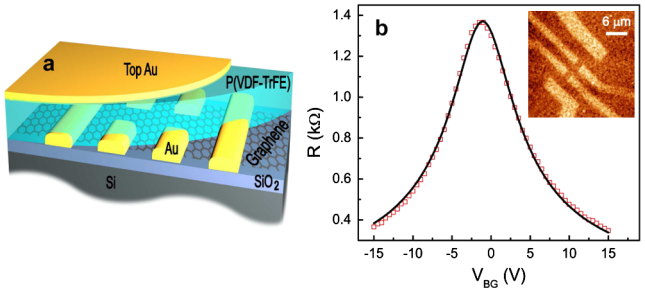

FIG. 1 (color online). (a) Sample geometry of GFeFETs. (b) R vs V_{BG} of one sample after PVDF coating. The red open square and black solid line are the experimental and fitting results, respectively. Inset: Atomic force microscopy of the sample after PVDF. Color scale: 0–164 nm.

The GFeFET sample geometry is shown in Fig. 1(a). Detailed sample fabrication procedures have been discussed in Ref. [16]. For the samples used in this study, the ferroelectric thin film of poly(vinylidene fluoride-trifluoroethylene 72:28) (PVDF) is $\sim$0.5 μm thick. The GFeFETs were electrically characterized at room temperature in vacuum by using the four-contact lock-in technique.

Before polarizing the ferroelectric, we first measured the Hall mobility and the resistance vs SiO_2 gate voltage characteristics (R vs V_{BG}) to determine the sample quality. Most samples retain their high mobility after PVDF spin-coating and annealing, as shown in Fig. 1(b) for a typical sample with Hall mobility of 4600 $\mathrm{cm^2\,V^{-1}\,s^{-1}}$ (see [17]). Quantitatively, the ambipolar R vs V_{BG} characteristics can be fitted very well by the model [19]:

$$R = \frac{L}{We\mu_{\mathrm{Hall}}\sqrt{n_{\mathrm{res}}^2 + n^2}}, \qquad (1)$$

by using the Hall mobility μ_{Hall}. For the sample shown in Fig. 1(b), the fitting yields a residual carrier concentration $n_{\mathrm{res}} = 2.77 \times 10^{11}\ \mathrm{cm^{-2}}$.

Compared to the SiO_2 gating, one fundamental difference introduced by ferroelectric gating is pronounced hysteresis in the resistance vs ferroelectric gate voltage characteristics (R vs V_{TG}). Though such hysteretic R vs V_{TG} can be qualitatively explained by the electric displacement continuity equation at the ferroelectric-graphene interface [16], a quantitative understanding of ferroelectric gating is still missing. Here, we introduce an independent n_{BG} using the SiO_2/Si back gate. This provides a well-defined, constant reference for determining the doping induced by PVDF gating. To study the effect of n_{BG} on the ferroelectric gating of GFeFETs, it is also important to limit the polarization magnitude in PVDF, since the effect of ferroelectric gating is nearly 10 times stronger than the SiO_2 gating [16]. Thus, we first introduced very small $|P_r|$ in PVDF by limiting the maximum top gate voltage ($V_{\mathrm{TG\,max}}$) to ± 5 V. Such low V_{TG} only slightly polarizes PVDF, allowing n_{BG} to match or even exceed the $|P_r|$-induced doping in graphene.

In Fig. 2(a), we show the resistance of the GFeFET as a function of both V_{TG} and V_{BG}. With $V_{\mathrm{BG}} \approx 6$ V, the R vs V_{TG} curve shows two symmetrical resistance peaks and nearly negligible $\Delta R/R$ [Fig. 2(b)(iii)]. By gradually tuning n_{BG} with V_{BG}, the two resistance peaks become more asymmetrical and shift leftward (rightward) for $n_{\mathrm{BG}} < 0$ ($n_{\mathrm{BG}} > 0$). The shift in peak positions leads to an increase in $\Delta R/R$, which has a maximum at $V_{\mathrm{BG}} \approx -6$ V [Fig. 2(b)(ii)] and $V_{\mathrm{BG}} \approx 18$ V [Fig. 2(b)(iv)], respectively. Crossing these two points, $\Delta R/R$ decreases as $|n_{\mathrm{BG}}|$ keeps on increasing. At large enough n_{BG}, the double peak structure eventually disappears in the R vs V_{TG} hysteresis [Figs. 2(b)(i) and 2(b)(v)].

The evolution of the resistance peaks and the change in $\Delta R/R$ can both be explained by two independent but competing doping processes in graphene by polarized ferroelectric dipoles and V_{BG}, respectively. For such a dual-gated system, the interfacial electric displacement continuity equation is expressed by

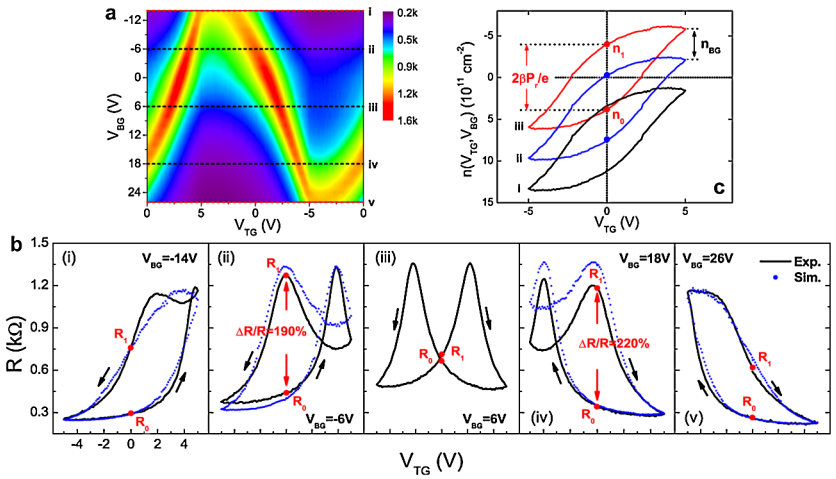

FIG. 2 (color online). (a) R vs V_{TG} and V_{BG} of the GFeFET with very small $|P_r|$. (b) Extracted single traces of R vs V_{TG} with different V_{BG}. The blue dotted lines are simulated results. (c) n_{BG} tunable doping hysteresis in GFeFETs. Only three doping hysteresis loops, corresponding to experimental curves (i), (ii), and (iii) in Fig. 2(b), are shown for clarity. See the main text for discussions.

$$-\beta P(V_{\mathrm{TG}}) + n^* = n(V_{\mathrm{TG}}, V_{\mathrm{BG}})e, \quad (2)$$

where $\beta P(V_{\mathrm{TG}})$ represents the hysteretic dipole doping by the ferroelectric gating [20] and $n^* = n_{\mathrm{env}} + n_{\mathrm{BG}}$ is the reference doping induced by the dielectric environment and V_{BG}, respectively. For $n^* \approx 0$, the doping in graphene is dominated by the ferroelectric gating by $n(V_{\mathrm{TG}}, n^* \approx 0) = -\beta P(V_{\mathrm{TG}})/e$. By using Eq. (1), it is now straightforward to see that $n(V_{\mathrm{TG}}, n^* \approx 0)$ will produce a R vs V_{TG} hysteresis with two symmetrical resistance peaks, centering on the two coercive-field points where $P(V_{\mathrm{TG}})$ crosses zero. Experimentally, this is the R vs V_{TG} curve in Fig. 2(b)(iii) with $V_{\mathrm{BG}} = 6$ V, in which two resistance peaks are centered at $V_{\mathrm{TG}} = \pm 2.2$ V, respectively. By converting each R in Fig. 2(b)(iii) into doping using Eq. (1), we directly determined the doping curve $n(V_{\mathrm{TG}}, n^* \approx 0)$. The result is shown in Fig. 2(c) (red curve). As expected, this doping curve is hysteretic and characterized by two zero-field doping levels with equal magnitude, i.e., $|n_1| = |n_0| = \beta P_r/e$.

After acquiring $n(V_{\mathrm{TG}}, n^* \approx 0)$, we can deduce individual $R(V_{\mathrm{TG}}, n^*)$ curves for nonzero n^* by substituting $n(V_{\mathrm{TG}}, V_{\mathrm{BG}}) = -\beta P(V_{\mathrm{TG}})/e + n_{\mathrm{env}} + \alpha V_{\mathrm{BG}}$ into Eq. (1). Here $\alpha = 7.2 \times 10^{10}\ \mathrm{cm^{-2}\,V^{-1}}$ is the doping coefficient of 300 nm SiO_2, and n_{env} is a fitting parameter (see [17]). By tuning n_{env} and matching the resistance peaks of the simulation to the experimental results, we simulated each experimental $R(V_{\mathrm{TG}}, V_{\mathrm{BG}})$ curve in Fig. 2(b). As shown by blue dotted lines, the simulation reproduces the evolution of the experimental results very well. Two resulting doping hysteresis for the resistance curves in Figs. 2(b)(i) and 2(b)(ii) are further compared with $n(V_{\mathrm{TG}}, n^* \approx 0)$ in Fig. 2(c). From the comparison, we can see that $\Delta R/R$ approaches the maxima as one zero-field doping level sits near the Dirac point when $|n^*| \approx \beta P_r/e$ (blue hysteresis loop). Further increase in n_{BG} moves *both* n_1 and n_0 away from the Dirac point, and $\Delta R/R$ decreases (black hysteresis loop).

Thus, we have shown that, by using a background doping introduced by normal dielectric gating as a reference, the hysteretic behavior of R vs ferroelectric gating in GFeFETs can be quantitatively determined by solving the electric displacement continuity equation. For memory applications, $\Delta R/R$ is of great importance. Following the above discussions, the two zero-field resistance states are $R_1 = L/We\mu\sqrt{n_{\mathrm{res}}^2 + (\beta P_r/e - n^*)^2}$ and $R_0 = L/We\mu\sqrt{n_{\mathrm{res}}^2 + (\beta P_r/e + n^*)^2}$, respectively. Thus, the best strategy to utilize the field-dependent resistance is to fully polarize the ferroelectric and introduce a matching n_{BG}, as demonstrated in Fig. 3(a). With $V_{\mathrm{TG\,max}} = 5$ V, two maxima of ~250% are present in $\Delta R/R$ vs V_{BG}, which can be also simulated very well by Eqs. (1) and (2) with $\beta P_r/e = 4.2 \times 10^{11}\ \mathrm{cm^{-2}}$. By increasing $V_{\mathrm{TG\,max}}$ to 30 V, the maximum $\Delta R/R$ is increased to 500%. The fast increase in P_r not only increases the maximum $\Delta R/R$, but also increases the separation between the two $\Delta R/R$ maxima, resulting in one maximum being outside of V_{BG} measurement range. For this $V_{\mathrm{TG\,max}}$, R vs V_{TG} shows a dominant double peak structure over the full V_{BG} range [Fig. 3(b)]. However, we can still see the tendency of a transition from double peak structure to single peak structure as V_{BG} exceeding 40 V.

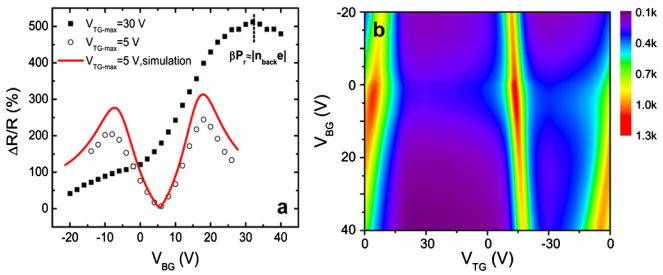

FIG. 3 (color online). (a) $\Delta R/R$ as a function of V_{BG} with different $V_{\mathrm{TG\,max}}$. Two maxima are observable with $V_{\mathrm{TG\,max}} = 5$ V (black open circles). The red solid line shows the simulation with $\beta P_r = 4.2 \times 10^{11}\ \mathrm{cm^{-2}}$. For $V_{\mathrm{TG\,max}} = 30$ V, the maximum $\Delta R/R$ is increased to 500% ($V_{\mathrm{BG}} = 32$ V). (b) R (V_{TG}, V_{BG}) of the GFeFET with higher βP_r ($\sim 2 \times 10^{12}\ \mathrm{cm^{-2}}$). Double peak structures dominate over the whole V_{BG} range.

Such n_{BG}-shifted hysteretic doping in graphene is a ferroelectric analogy to the ferromagnetic exchange bias [18]. Utilizing this electrostatic effect, the bit writing in GFeFETs can be much simplified by switching the ferroelectric polarization between P_r and $-P_r$, by using symmetrical voltage sweeps. With $n_{\mathrm{BG}} \approx -\beta P_r/e$, to write the high resistance "1," a negative writing voltage ($-V_{\mathrm{writing}}$) is applied to the ferroelectric, setting the dipole polarization to $-P_r$ independent of the initial states in the unit cell [Figs. 4(a) and 4(b)]. In contrast, a positive V_{writing} with the same magnitude sets the GFeFET into low resistance "0" [Figs. 4(c) and 4(d)]. Compared to the asymmetrical bit writing by polarizing and depolarizing the ferroelectric alternately [16], such symmetrical writing in GFeFETs not only provides simplicity but also takes full advantage of the fast switching speed of the ferroelectric. For lead zirconate titanate based materials, this can be as fast as 280 ps [21]. Another potential application of this electrostatic effect could be *multibit-per-cell* data storage in GFeFETs utilizing the n_{BG} tunable $\Delta R/R$.

We have also tested the reproducibility of our GFeFETs working with $\beta P_r \approx |n^*|e$. During the fatigue test, a triangular wave of 1 kHz was applied to the PVDF thin film. Every 12 (24) seconds, the triangular wave was interrupted, and one R vs V_{TG} curve was recorded. The corresponding $\Delta R/R$ as a function of switching cycles and the raw data of individual R vs V_{TG} curves are summarized in Figs. 4(e) and 4(f), respectively. The fatigue test clearly demonstrates reproducible nonvolatile switching exceeding 100 k cycles in the GFeFET. Ultimately, the life span of PVDF-based GFeFETs is 10^7 [22]. Thus, PVDF-GFeFETs could provide a cost-effective solution for flexible nonvolatile data storage with submicrosecond switching speed. On the other hand, inorganic ferroelectric (such as lead zirconate

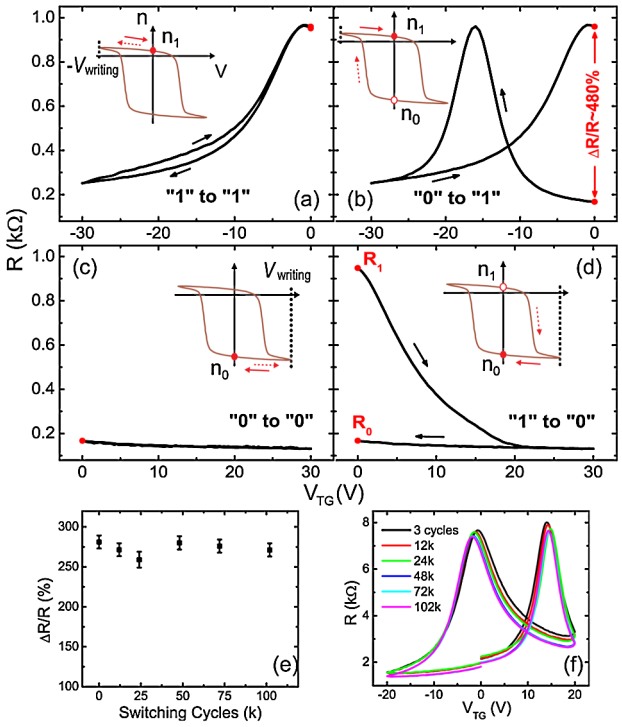

FIG. 4 (color online). Symmetrical bit writing in GFeFETs with $n_{BG} \approx -\beta P_r/e$. (a),(b) Writing 1 by using $-V_{writing}$. (c), (d) Writing 0 by using $V_{writing}$. Dashed and solid arrows indicate the forward and backward voltage sweep directions, respectively. The writing is independent on the initial states. (e), (f) Fatigue test of one GFeFET with symmetrical bit writing, showing nonvolatile switching cycles exceeding 100 k.

titanate) should be used if fast writing speed ($<$ ns) and ultrahigh endurance (10^{10}) are required.

In conclusion, we have demonstrated a quantitative way of determining and controlling the hysteretic ferroelectric gating in GFeFETs. By using an independent linear dielectric gating (n_{BG}) as a reference [23], ferroelectric gating can be quantitatively determined by the electric displacement continuity equation. The reference gating can also be used to control ferroelectric gating by introducing a unidirectional shift in the hysteretic ferroelectric doping in GFeFETs. One specific application of this electrostatic ''bias'' effect is symmetrical bit writing in GFeFETs directly utilizing P_r and $-P_r$ with speed and simplicity. The ferroelectric gating phenomena and related modeling and controlling methods presented in this study will be important in understanding future charge transport studies on ferroelectric gated graphene electronic devices.

We particularly acknowledge Douwe J. Monsma for many insights and useful discussions. This work is supported by the Singapore National Research Foundation Grants No. NRF-RF2008-07 and NRF-CRP (R-143-000-360-281), a NUS/SMF grant, the U.S. Office of Naval Research (ONR and ONR Global), and NUS NanoCore.

*Corresponding authors.
†phyob@nus.edu.sg

[1] A. K. Geim and K. S. Novoselov, Nature Mater. **6**, 183 (2007); A. H. Castro Neto *et al.*, Rev. Mod. Phys. **81**, 109 (2009).
[2] K. S. Novoselov *et al.*, Nature (London) **438**, 197 (2005); Y. Zhang *et al.*, *ibid.* **438**, 201 (2005).
[3] M. I. Katsnelson, K. S. Novoselov, and A. K. Geim, Nature Phys. **2**, 620 (2006); A. F. Young and P. Kim, *ibid.* **5**, 222 (2009).
[4] E. V. Castro *et al.*, Phys. Rev. Lett. **99**, 216802 (2007); Y. B. Zhang *et al.*, Nature (London) **459**, 820 (2009).
[5] J. González, F. Guinea, and M. A. H. Vozmediano, Phys. Rev. Lett. **84**, 4930 (2000).
[6] Y. Hatsugai, T. Fukui, and H. Aoki, Phys. Rev. B **74**, 205414 (2006).
[7] J. González, Phys. Rev. B **78**, 205431 (2008).
[8] B. Valenzuela and M. A. H. Vozmediano, New J. Phys. **10**, 113009 (2008).
[9] V. M. Pereira and A. H. Castro Neto, Phys. Rev. Lett. **103**, 046801 (2009).
[10] T. Ando, J. Phys. Soc. Jpn. **75**, 074716 (2006).
[11] J. H. Chen *et al.*, Nature Nanotech. **3**, 206 (2008).
[12] X. Hong *et al.*, Phys. Rev. Lett. **102**, 136808 (2009).
[13] L. A. Ponomarenko *et al.*, Phys. Rev. Lett. **102**, 206603 (2009).
[14] K. I. Bolotin *et al.*, Phys. Rev. Lett. **101**, 096802 (2008); X. Du *et al.*, Nature Nanotech. **3**, 491 (2008).
[15] A. Das *et al.*, Nature Nanotech. **3**, 210 (2008).
[16] Y. Zheng *et al.*, Appl. Phys. Lett. **94**, 163505 (2009).
[17] See supplemental material at http://link.aps.org/supplemental/10.1103/PhysRevLett.105.166602 for electron-hole puddles in GFEFETs and the Landau-Devonshire theory of ferroelectrics.
[18] J. Nogués *et al.*, Phys. Rep. **422**, 65 (2005).
[19] S. Kim *et al.*, Appl. Phys. Lett. **94**, 062107 (2009).
[20] β represents the electric coupling between ferroelectric dipoles and graphene, which is 1 for an ideal ferroelectric-graphene interface. For the GFeFETs in this study, the charge carrier doping in graphene after fully polarizing the ferroelectric is $\sim 3 \times 10^{13}$ cm^{-2}, which is 40% lower than the ideal doping of $\sim 5 \times 10^{13}$ cm^{-2}.
[21] M. Dawber, K. M. Rabe, and J. F. Scott, Rev. Mod. Phys. **77**, 1083 (2005).
[22] T. Furukawa, T. Nakajima, and Y. Takahashi, IEEE Trans. Dielectr. Electr. Insul. **13**, 1120 (2006).
[23] n_{BG} can be precisely controlled by preparing graphene on ferroelectrics and introducing fixed molecular doping. An alternative way is using epitaxial graphene on SiC.